TOWARDS A MODULAR APPROACH FOR UNSTRUCTURED SHOCK-FITTING

R. Pepe [1], A. Bonfiglioli[1], R. Paciorri[2], A. Lani[3], J. G. Mena[3] C. F. Olliver-Gooch[4]

[1] Università della Basilicata , 85100, Potenza, Italy aldo.bonfiglioli@unibas.it
[2] Università di Roma, 00184, Roma, Italy, renato.paciorri@uniroma1,it
[3] von Karman Institute, 1640 Sint-Genesius-Rode, Belgium, lani@vki.ac.be
[4] University of British Columbia, V6T 1Z4, Vancouver, Canada, cfog@mech.ubc.ca

Key words: Hypersonic flows, thermochemical nonequilibrium flows, shock-capturing, shock-fitting, unstructured meshes.

Abstract. We present a modular shock-fitting algorithm for unstructured grids that can be used in conjunction with virtually any vertex-centred shock-capturing solver. The unstructured, shock-fitting algorithm, originally developed for ideal gases, has here been extended to thermochemical nonequilibrium flows and coupled with *COOLFluiD*, an in-house shock-capturing CFD solver developed at the Von Karman Institute. Results obtained in the computation of hypersonic flows past circular cylinders are presented for both ideal gas and dissociating Nitrogen in thermochemical nonequilibrium.

1 INTRODUCTION

The accurate simulation of hypersonic flows past blunt bodies using unstructured grids is still a challenge, despite more than 20 years of algorithmic developments on unstructured shock-capturing solvers. Indeed, the numerical modelling of strong bow shocks, shock-shock and shock-boundary layer interaction, that invariably occur in a typical hypersonic flow, can heavily affect the accuracy of the entire flowfield. Widespread "traditional" shock-capturing solver often exhibit severe drawbacks when used to simulate hypersonic flows: stagnation point anomalies [1], carbuncle and spurious oscillations [2] and a reduction of the order of accuracy within the entire shock-downstream region [3]. These drawbacks seem to be caused by the numerical details of the capturing process, so that shifting to an entirely different numerical modeling of the discontinuities might prove useful.

The shock-fitting approach, which has been made popular since the mid 60s by Moretti and collaborators [4], has already proved to be immune to the shock-capturing drawbacks. Shock-fitting consists in using the Rankine-Hugoniot jump relations to explicitly track the motion of the discontinuities in a Lagrangian manner.

Shock-fitting algorithms have been used in the past to simulate chemically reacting nonequilibrium flows on structured grids, see e.g. the work by Pfitzner [5] and Paciorri et. al. [6] in the 90s. More recently, Prakash et al. [7] have developed an high order finite difference shock-fitting algorithm to simulate thermochemical nonequilibrium flows on structured grids. In recent years, some of the authors [8, 9, 10, 11] have developed an unstructured shock-fitting algorithm which is algorithmically simpler than the shock-fitting algorithms traditionally used in the structured-grid setting. In the present contribution, the unstructured shock-fitting algorithm has been has been extended to deal with thermochemical nonequilibrium flows and coupled with *COOLFluiD* [16, 17], an in-house CFD solver developed at the Von Karman Institute (VKI). Results have been obtained for both ideal and thermochemical nonequilibrium inviscid flows.

2 GOVERNING EQUATIONS

2.1 Governing equations

The system of equations considered in this work is the set of Euler equations governing multispecies and two-temperature flows:

$$\frac{\partial \mathbf{U}}{\partial t} + \nabla \cdot \mathbf{F}^c = \mathbf{S}, \tag{1}$$

where $\mathbf{U}$ stands for the conservative variables vector, $\mathbf{F}^c$ for the convective flux tensor and $\mathbf{S}$ for the source terms vector. For a 2 temperature, multispecies flow, the conservative variables vector includes the species densities ρ_i, the momentum $\rho\mathbf{u}$, the total energy ρE and the vibrational energy ρe_v:

$$\mathbf{U} = \left[\ \rho_i, \quad \rho\mathbf{u}, \quad \rho E, \quad \rho e_v\ \right]^t. \tag{2}$$

The components of the convective flux tensor $\mathbf{F}^c$ are given in Eq. (3):

$$\mathbf{F}^c = \left[\ \rho_i\mathbf{u}, \quad \rho\mathbf{u}\mathbf{u} + pI_{d\times d}, \quad \rho\mathbf{u}H, \quad \rho\mathbf{u}e_v\ \right]^t, \tag{3}$$

where p is the pressure, H the total enthalpy and $I_{d\times d}$ is the identity matrix of order d.
The source term vector $\mathbf{S}$ is given by:

$$\mathbf{S} = \left[\ S_{\rho_i}, \quad \mathbf{0}^t, \quad 0, \quad S_{e_v}\ \right]. \tag{4}$$

Chemical source terms S_{ρ_i} in Eq. (4) are given by the mass action law:

$$S_{\rho_i} = M_i \sum_{r=1}^{N_r} \left(\nu_{ir}^{''} - \nu_{ir}^{'} \right) \dot{\xi}_r, \qquad (5)$$

where $\dot{\xi}_r$ is the velocity for the rth chemical reaction:

$$\dot{\xi}_r = k_{fr} \prod_{i=1}^{N_s} \left(\frac{\rho_i}{M_i} \right)^{\nu_{ir}^{'}} - k_{br} \prod_{i=1}^{N_s} \left(\frac{\rho_i}{M_i} \right)^{\nu_{ir}^{''}}. \qquad (6)$$

In Eqs. (5 - 6) N_s is the number of chemical species, N_r the number of chemical reactions, M_i the molar weight of the ith species, k_{fr} and k_{br} resp. the forward and backward reaction rates and $\nu_{ir}^{'}$ and $\nu_{ir}^{''}$ resp. the stoichiometric coefficients of the products and the reagents. The vibrational energy source term $\dot{S}_{e^v}$ accounts for the energy exchange between the roto-translational and the vibrational modes:

$$\dot{S}_{e^v} = \sum_{i=1}^{N_s} \rho_i \frac{(e_{v,s}(T) - e_{v,s}(T_v))}{\tau_s}, \qquad (7)$$

where $e_{v,s}$ is the specific vibrational energy and τ_s is the relaxation time of the sth species; T is the rototraslational temperature and T_v the vibrational temperature. More details concerning the thermochemical model implemented in *COOLFluiD* can be found in [20, 19, 21]. The thermochemical properties are provided by the MUTATION [31] library developed at the VKI.

When dealing with an inert gas, the governing PDEs are only given by the continuity equation for the single gas, the linear momentum conservation equation and the conservation equation of total energy. The conservation equation of the vibrational energy is neglected and there are no source term contributions in the governing equations.

3 COMPUTATIONAL TOOLS

3.1 Shock-fitting technique

The unstructured shock-fitting algorithm that has been recently developed by some of the authors [8, 9, 10, 11] consists of two key ingredients: *i*) a local re-meshing technique that constructs a time-dependent mesh in which the fitted discontinuities are internal boundaries of zero thickness and *ii*) an algorithm for solving the Rankine-Hugoniot jump relations that provides the Lagrangian velocity of the discontinuity and an updated set of dependent variables within the downstream side of the fitted shock. More precisely, in two space dimensions the fitted shock fronts are made of polygonal curves, i.e. a connected series of line segments (which we call the shock edges) that join the shock points. Two sets of flow states, corresponding to the upstream and downstream sides of the discontinuity,

are assigned to each of the shock-points located on either side of the shock front. The downstream state and the shock speed are computed according to the Rankine-Hugoniot jump relations and the fitted shock is allowed to move throughout a background triangular mesh that covers the entire computational domain.

Local re-meshing around the shock is accomplished using public domain software: `triangle` [13] in 2D and `tetgen` [14] and `yams` [15] in 3D. In the near future, we plan to accomplish this same task using the local remeshing technique designed by Zaide and Olliver-Gooch [18].

The fitted shocks are treated as interior boundaries by the same shock-capturing code which is used to solve the discretised governing equations in the smooth regions of the flow-field.

Recently, the shock-fitting algorithm, originally developed for an ideal gas, has been extended to chemical non-equilibrium flows [23]. The generalization to a reactive mixture has required a minimum effort, since modeling the bow shock as a partly dispersed shock wave [22], the concentrations of chemical species are kept frozen while passing through the bow shock.

When dealing with thermochemical non-equilibrium, as we do in the present work, the specific vibrational energy is kept constant through the bow shock.

3.2 Shock-capturing solver

One of the key features of the unstructured shock-fitting algorithm is its modularity: the shock-capturing code used to discretise the governing PDEs (1) in the smooth regions of the flowfield is used as a "black box" by the shock-fitting algorithm. The only constraint is that the unstructured shock-capturing solver must feature a vertex-centred storage of the unknowns. In [8, 9, 10, 11] the unstructured shock-fitting algorithm had been coupled with the in-house `eulfs` [12] shock-capturing code. In the present work, the shock-capturing solver has been replaced, with a very limited coding effort, with the VKI-developed *COOLFluiD* [16, 17] solver. This was done both for demonstrating the modularity of the unstructured shock-fitting algorithm, but also because *COOLFluiD* features a wider range of modelling capabilities than `eulfs`. Both codes use Residual Distribution schemes (*RD*) [1] for the spatial discretization, so we briefly introduce the main characteristics of the *RD* discretization for the governing PDEs (1); further details can be found, e.g. in [24, 25].
The solution is expressed by means of a Finite Element *FE* linear representation:

$$\mathbf{U}^h(\mathbf{x}, t) = \sum_j \mathbf{U}_j N_j(\mathbf{x}), \tag{8}$$

where the *FE* linear shape function $N_j(\mathbf{x}_k) = \delta_{jk}$ has a tent-like shape and thus takes

---

[1]*RD* schemes are also known under the name of Fluctuation Splitting schemes (FS).

value 1 at grid point j and 0 within its distance-1 neighbours.

For each element e with volume Ω_e and boundary surface $\partial\Omega_e$, the steady-state residual is defined by:

$$\mathbf{\Phi}^e = \oint_{\partial\Omega_e} \mathbf{F} \cdot \mathbf{n} dS - \int_{\Omega_e} \mathbf{S} dV = \mathbf{\Phi}^{c,e} - \mathbf{\Phi}^{S,e}. \tag{9}$$

Since the dependent variables are associated with the grid-points of the computational mesh, a nodal residual needs to be constructed within each mesh-point. The nodal residual is then assembled by collecting fractions $\mathbf{\Phi}_i^{c,e}$, resp. $\mathbf{\Phi}_i^{S,e}$, of the net inviscid fluxes $\mathbf{\Phi}^{c,e}$, resp. the volumetric integral of the source term $\mathbf{\Phi}^{S,e}$, associated with all the elements e by which the node i is surrounded:

$$\mathbf{\Phi}_i^c = \sum_{i \ni e} \mathbf{\Phi}_i^{c,e}, \qquad \mathbf{\Phi}_i^S = \sum_{i \ni e} \mathbf{\Phi}_i^{S,e}. \tag{10}$$

The convective contribution to the nodal residual is generally expressed as:

$$\mathbf{\Phi}_i^c = \sum_{i \ni e} \mathbf{B}_i^e \mathbf{\Phi}^{c,e} \tag{11}$$

where $\mathbf{B}_i^e$ are the so called distribution matrices, which define the cell residual fraction of the element e which is sent to its vertex i. The distribution matrices depend on the nodal upwind parameters:

$$K_j = \frac{1}{d} \sum_{i=1}^{d} \mathbf{A}_{j,x_i} n_{j,x_i} \tag{12}$$

where $\mathbf{A}_{j,x_i}$ is the Jacobian of the convective flux projected along the direction x_i and n_{j,x_i} are the components of the vectors normal to the element faces. When dealing with perfect gases, the Jacobian matrices are computed by means of a conservative linearization based on Roe's parameter vector [26, 27].

It is possible to construct schemes that depend linearly upon the solution (when solving a linear PDE) and are either monotonicity preserving, but limited to first order of accuracy, which is the case of the N scheme, or, if second order accurate, may lead to oscillatory behaviour in the neighbourhood of a captured discontinuity, which is the case of the LDA scheme:

$$\mathbf{\Phi}_i^{e,N} = K_i^+ \cdot \left(\mathbf{U}_i - \mathbf{U}_{inlet}^e \right), \qquad \mathbf{\Phi}_i^{e,LDA} = \mathbf{B}_i^{e,LDA} \mathbf{\Phi}^e.$$

The *inlet* state $\mathbf{U}^e_{inlet}$ and *LDA* distribution matrix $\mathbf{B}^{e,LDA}_i$ are given by:

$$\mathbf{U}^e_{inlet} = \sum_{j=1}^{d+1} \left(K_j^-\right)^{-1} \cdot \sum_{j=1}^{d+1} K_j^- \cdot \mathbf{U}_j, \qquad \mathbf{B}^{e,LDA}_i = K_i^+ \cdot \left(\sum_{j=1}^{d+1} K_j^+\right)^{-1}.$$

Monotone and second-order-accurate schemes can be obtained by blending the linear N and *LDA* schemes with an element-wise matrix $\mathbf{\Theta}^e$:

$$\mathbf{\Phi}^{e,B}_i = \mathbf{\Theta}^e \mathbf{\Phi}^{e,N}_i + (\mathbf{I} - \mathbf{\Theta}^e) \mathbf{\Phi}^{e,LDA}_i \tag{13}$$

These kind of non-linear schemes (the matrix $\mathbf{\Theta}^e$ depends upon the local solution) are referred to as B schemes.

For thermochemical nonequilibrium flows, a conservative linearization is not available and therefore a different approach, named Conservative Residual Distribution (CRD) [2] is used. This kind of approach consists in calculating the flux integral by means of numerical quadrature, thus avoiding the conservative linearization. Details on this specific issue can be found in [28, 29]. The source terms residual is distributed in the same manner as the convective residual.

After having applied the RD spatial discretization to the governing PDEs, one obtains the following system of ODEs governing the pseudo-temporal evolution of the solution at the node i:

$$V_{\Omega_i} \frac{\mathrm{d}\mathbf{U}}{\mathrm{d}t} + \mathbf{\Phi}^c_i - \mathbf{\Phi}^S_i = \mathbf{0} \tag{14}$$

where V_{Ω_i} is the volume of the median dual cell surrounding the node i.
Equation (14) is marched in pseudo-time until a steady state solution is reached using a an implicit backward Euler integrator. The linear system is solved using one of the iterative, preconditioned Krylov subspace algorithms available in the `PETSc` library [30].

4 RESULTS AND DISCUSSIONS

4.1 Hypersonic flow of an ideal gas past a circular cylinder

An hypersonic inviscid flow past a circular cylinder at freestream Mach number, $M_\infty = 20$, has been considered as a first test case. Results for this same test case had already been obtained by some of the authors [8] using the `eulfs` solver. Two different grids with increasing spatial resolution have been used: they are shown in Fig. 1 while the

---

[2] CRD variants of the RD schemes are identified by a c character appended to the name of the scheme (example $LDAc$).

number of triangles and nodes are reported in Tab. 4.1. The shock-fitted grids differ from the corresponding background ones because of the addition of the shock points; the background grids have also been used for the calculations in which the shock is captured. All the results obtained for the ideal inviscid gas flows have been carried out by means of an explicit backward Euler time integration scheme.

Table 1: Characteristics of the grids used for the inviscid hypersonic flow over a circular cylinder.

	coarse grid		fine grid	
	Nodes	Elements	Nodes	Elements
Background grid	351	610	5261	10151
Shock-fitted grid	411	654	5415	10229
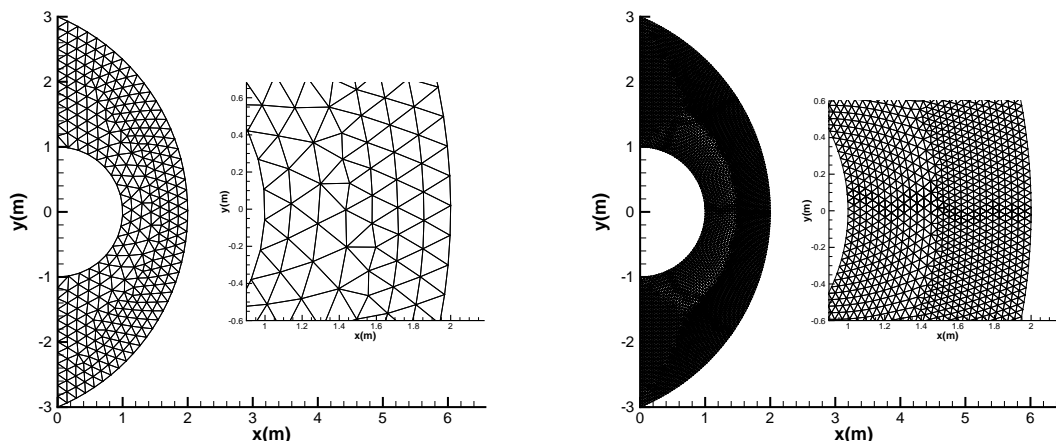
Figure 1: Coarse grid (*left*) and fine grid (*right*).

The comparison between the shock-capturing and shock-fitting results is shown in Fig. 2, where pressure contour plots are shown for both the coarse and the fine grid solutions. The non-linear B scheme has been used to obtain a nominally second-order-accurate solution when the shock is captured, whereas the linear LDA scheme has been used in the shock-fitting calculation. The use of a linear scheme in the shock-fitting calculation is made possible by the fact that, when all shocks are fitted, the LDA scheme is used only in smooth regions of the flow field.
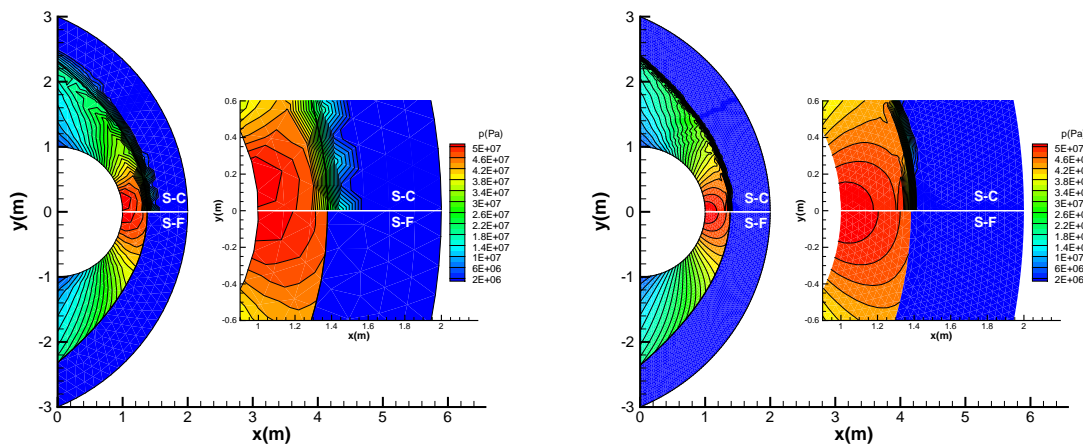
Figure 2: Pressure contour plot: comparison between the shock-fitting and shock-capturing second-order-accurate accurate solutions obtained on the coarse (*left*) and the fine grid (*right*).

Figure 2 clearly shows that, using grids of comparable resolution, shock-fitting not only avoids smearing the shock, but it also allows to obtain a much cleaner solution within the entire shock layer characterized by a low numerical error also on the coarse mesh. It is worth to observe that the shock-capturing solution computed on the coarse mesh features a strong asymmetry with respect to the stagnation point, whereas this asymmetry is completely absent in the shock-fitting solution computed on the corresponding coarse mesh.

Finally, the results obtained for this same test-case by coupling the two different CFD solvers, *COOLFluiD* and `eulfs`, with the same shock-fitting code, have been compared in Fig. 3, where pressure iso-contour lines are displayed for both the fist-order-accurate N and second-order-accurate *LDA* schemes. Not surprisingly, the results are superimposed since the two codes implement the same FS discretization schemes.

4.2 Thermochemical nonequilibrium flow over a circular cylinder

The nonequilibrium shock-fitting algorithm has been tested by reference to the flow conditions of Hornung's experiment [32], listed in Tab. 4.2. The grid used is a obtained by a 120×120 structured mesh cutting into two triangles each quadrilateral. The triangulation is symmetric in the stagnation region, as shown in Fig. 4. The background mesh is made of 14884 nodes and 29282 elements, the shock-fitting grid at steady-state, which differs from the background triangulation only in the neighbourhood of the fitted shock, has 15039 nodes and 29371 elements.

The numerical simulations were carried out for inviscid flow, since the purpose of this study is to asses the capability of the unstructured shock-fitting technique to correctly predict the shock position on blunt bodies in the case of thermochemical nonequilibrium
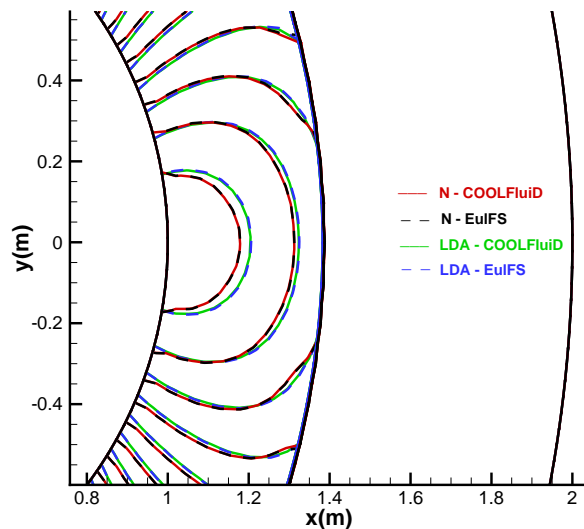
Figure 3: Pressure contour plot for the shock fitting solutions: comparison between *COOLFluiD* and `eulfs` solutions.

flows. Since the PDEs governing dissociating nitrogen can be very stiff, it has been necessary to use the implicit backward Euler scheme to obtain the steady-state solution. As shown in Fig. 5, the shock-wall distance agrees reasonably well with the experimental results obtained by Hornung. In Fig. 6 the pressure contour plot computed using the first-order-accurate *Nc* scheme is compared with the one obtained by Wang and Zhong [33] using a third-order-accurate finite difference shock fitting scheme on structured meshes. The good agreement between the two solutions obtained by the two different schemes with different order of accuracy proves that both the solutions are grid-independent, i.e. characterized by a very low numerical error.

Table 2: Freestream conditions for a nitrogen flow around a 1 *inch* radius cylinder.

Physical quantity	M_∞	p_∞ [Pa]	T_∞ [K]	$T_{v\infty}$ [K]	u_∞ [m/s]	$\alpha_{N\infty}$
Free-stream Value	6.13	2908.0	1833.0	1833.0	5594.0	0.07
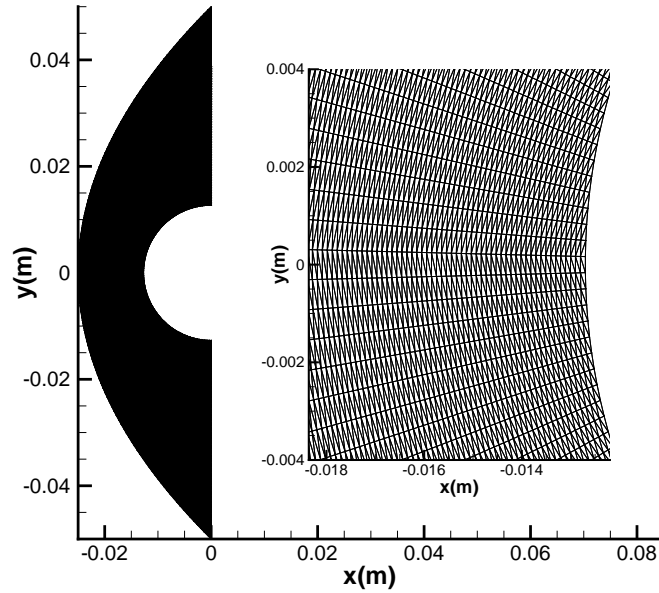
Figure 4: Grid used for the Nitrogen flow over a circular cylinder.
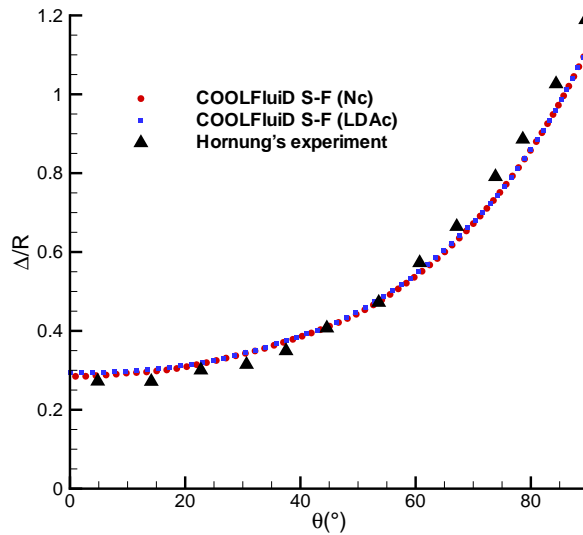
Figure 5: Non-dimensional shock-wall distance: $COOLFluiD + SF$ vs. Hornung's experimental measurements. θ is the azimuthal angle which takes value 0 at the stagnation point, Δ/R is the shock-wall distance divided by the cilinder's radius.

10
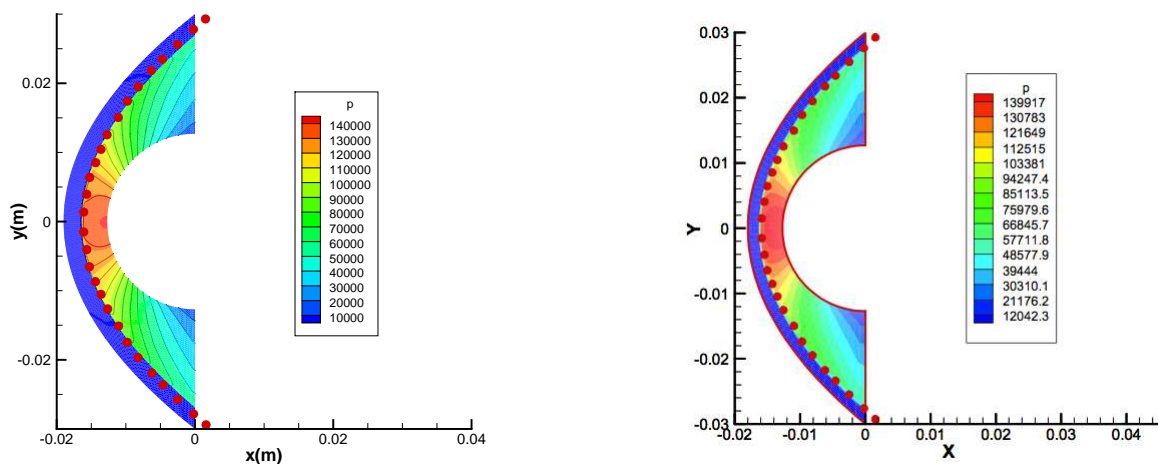
Figure 6: Pressure contour plot: *COOLFluiD + SF* (*left*) vs. ref. [33] (*right*). Hornung's experimental measurements of the shock standoff distance are represented by the red circles.

5   CONCLUSIONS

A modular shock-fitting algorithm for unstructured meshes was coupled with the VKI's COOLFluiD code. This operation demonstrated the high modularity of the unstructured shock-fitting algorithm and, in the same time, allowed a complete extension of the proposed shock-fitting to thermochemical non-equilibrium flows.

The resulting code was tested on several high speed flows past a circular cylinder assuming the working gas as a perfect gas and as a real gas in thermochemical non-equilibrium. Results confirm that shock-fitting not only allows a better modelling of the bow shock providing a good estimate of the position of the bow shock, but also improves the solution quality within the entire shock-layer.

REFERENCES

[1] P. A. Gnoffo and J. A. White, *Computational Aerothermodynamic Simulation Issues On Unstructured Grids*, 37th AIAA Aerospace Science Meeting and Exhibit, AIAA, Portland, 2004.

[2] K. Kitamura, E. Shima, Y. Nakamura and P. L. Roe, Evaluation of Euler fluxes for hypersonic flow computations, *AIAA Journal*, Vol. 48, No. 4, 763776, 2010.

[3] M. H. Carpenter and J. H. Casper, Accuracy of Shock Capturing in Two Spatial Dimensions, *AIAA Journal*, Vol. 37, No. 9, 10721079, 1999.

[4] G. Moretti and M. Abbett, A time-dependent computational method for blunty body flows, *AIAA Journal*, Vol. 4, No. 12, 2136-2141, 1966.

[5] M. Pfitzner, *A 3-D non-equilibrium shock-fitting algorithm using effective RankineHugoniot relations*, AIAA, 22nd Fluid Dynamics, Plasma Dynamics and Lasers Conference, Honolulu, 1991.

[6] R. Paciorri, F. Sabetta, B. Favini, On the Role of Vibrational Excitation in Hypersonic Flow Computations, *Meccanica* , Vol. 33, 331347, 1998.

[7] A. Prakash, N. Parsons, X. Wang and and X. Zhong, High-order shock-fitting methods for direct numerical simulation of hypersonic flow with chemical and thermal nonequilibrium, *Journal of Computational Physics*, Vol. 230, No. 23, 8474 8507, 2011.

[8] R. Paciorri and A. Bonfiglioli. A shock-fitting technique for 2D unstructured grids. *Computers and Fluids* Vol.38,no.3,715–726, 2009.

[9] R. Paciorri and A. Bonfiglioli. Shock interaction computations on unstructured, two-dimensional grids using a shock-fitting technique. *Journal of Computational Physics* Vol.230, no.8, 3155–3177, 2011.

11

[10] M. Ivanov, A. Bonfiglioli, R. Paciorri and F. Sabetta. Computation of Weak Steady Shock Reflections by means of an Unstructured Shock-Fitting Solver. *Shock Waves*, 271-284, 2010.

[11] A. Bonfiglioli and M. Grottadaurea and R. Paciorri and F. Sabetta. An unstructured, three-dimensional, shock-fitting solver for hypersonic flows. *Computers and Fluids* Vol.73,no.0,162–174, 2013.

[12] A. Bonfiglioli. Fluctuation splitting schemes for the compressible and incompressible Euler and Navier-Stokes equations. *International Journal of Computational Fluid Dynamics* Vol.14, no.1, 21–39, 2000.

[13] J. R. Shewchuk. Triangle: Engineering a 2D Quality Mesh Generator and Delaunay Triangulator. *Lecture Notes in Computer Science* Vol.1148,203–222, 1996.

[14] H. Si. TetGen a quality tetrahedral mesh generator and a 3D Delaunay triangulator. 2011. http://tetgen.berlios.de/.

[15] P.J. Frey. Yams: a fully automatic adaptive isotropic surface remeshing procedure. *Rapport technique n° 0252*, Institut National de Recherche en Informatique et en Automatique (I.N.R.I.A.) ISSN 0249-0803, 2001, http://www.ann.jussieu.fr/ frey/software.html.

[16] A. Lani and T. Quintino and D. Kimpe and H. Deconinck, *The COOLFluiD Framework - Design Solutions for High-Performance Object Oriented Scientific Computing Software*, ICCS 2005, Atlanta (GA), LNCS 3514, Vol.1, pp. 281-286, Springer-Verlag, 2005.

[17] A. Lani and N. Villedieu and K. Bensassi and L. Kapa and M. Panesi and M. S. Yalim , *COOLFluiD: an open computational platform for multi-physics simulation*, 21st AIAA CFD Conference, AIAA 2013-2589, San Diego, 2013.

[18] D. W. Zaide and C. F. Ollivier-Gooch. Inserting a Curve into an Existing Two Dimensional Unstructured Mesh. *Proceedings of the 22nd International Meshing Roundtable* ,93-107, 2014.

[19] R. K. Prabhu. An implementation of a chemical and thermal nonequilibrium flow solver on unstructured meshes and application to blunt bodies,*NASA Contractor Report*, 194967, 1994.

[20] P. A. Gnoffo, R. N. Gupta and J. L. Shinn. Conservation equations and physical models for hypersonic air flows in thermal and chemical nonequilibrium, *NASA Technical Paper*, 2867, 1989.

[21] C. Park. Nonequilibrium Hypersonic Aerothermodynamics,, John Wiley and Sons, New York, 1989.

[22] W. G. Vincenti and C. H. Kruger. Introduction to physical gas dynamics, John Wiley and Sons, 1965.

[23] R. Pepe, A. Bonfiglioli, A. D'Angola, G. Colonna and R. Paciorri , *An unstructured solver for argon plasma flows with reduced state-to-state kinetics*, 21st AIAA CFD Conference, AIAA 2013-3004, San Diego, 2013.

[24] E. van der Weide, Compressible flow simulation on unstructured grids using multi-dimensional upwind schemes, *Ph.D. thesis*, Technische Universitet Delft, 1998.

[25] M. Ricchiuto Construction and analysis of compact residual distribution discretizations for conservation laws on unstructured meshes, *Ph.D. thesis*, Université Libre de Bruxelles, 2005.

[26] P. L. Roe, Approximate Riemann Solvers, Parameter Vectors, and Difference Schemes,*Journal of Computational Physics*, vol. 43 (2), 357-372, 1981.

[27] H. Deconinck, P. L. Roe,R. Struijs, A multidimensional generalization of Roe's flux difference splitter for the Euler equations, *Computer & Fluids*, Vol. 22, 215-222, 1993.

[28] A. Csik, M. Ricchiuto, H. Deconinck, A Conservative Formulation of the Multidimensional Upwind Residual Distribution Schemes for General Nonlinear Conservation Laws, *Journal of Computational Physics*, Vol. 179, No. 1, 286 312, 2002.

[29] A. Lani and H. Deconinck, *Conservative Residual Distribution Method for Hypersonic Flows in Thermochemical Nonequilibrium*, 47th AIAA Aerospace Sciences Meetings, AIAA 2009-460, Orlando, 2009.

[30] S. Balay, J. Brown, K. Buschelman, V. Eijkhout, W: D. Gropp, D. Kaushik, M. G. Knepley, L. C. McInnes, B. F. Smith, H. Zhang, PETSc userrs manual, Thech. Rep. ANL-95/11 - Revision 3.4, Argonne National Laboratory, 2013.

[31] M. Panesi Physical models for nonequilibrium plasma flow, *PhD thesis*, Universitá degli studi di Pisa, 2009.

[32] H. G. Hornung, Non-equilibrium dissociating nitrogen flow over spheres and circular cylinder, *Journal of Fluid Mechanics*, Vol. 53(1), 149-176, 1972.

[33] X. Wang and X. Zhong, *A High-Order Shock-Fitting Non-Equilibrium Flow Solver for DNS of Strong Shock and Turbulence Interactions*, 7th International Conference on Computational Fluid Dynamics, ICCFD7-2305, Big Island, Hawaii, 2012.